Journal of Inflammation Research

Dovepress
Taylor & Francis Group

Open Access Full Text Article

ORIGINAL RESEARCH

Deacetyl Ophiopojaponin A ameliorates Asthma by Inhibiting L-Type Calcium Channel Cav2.3 to Reduce Calcium Load in Airway Epithelial Cells

Huan Li[1,*], Lingxue Jiang[1,*], Jing Qian[2,*], Wenping Bao[3], Kenan Huang[4], Dongyun Li[1], Aihua Zhang[5], Jianguo Sun[6], Jialong Lu[1], Danxia Wei[1]

[1]Department of Nephrology and Rheumatology, The Third Affiliated Hospital of Yunnan University of Traditional Chinese Medicine, Kunming, Yunnan, People's Republic of China; [2]Department of Rehabilitation, Second Affiliated Hospital of Naval Medical University, Shanghai, People's Republic of China; [3]Department of Traditional Chinese Medicine, Dounan Community Health Service Center of Chenggong District, Kunming, Yunnan, People's Republic of China; [4]Department of Thoracic Surgery, Second Affiliated Hospital of Naval Medical University, Shanghai, People's Republic of China; [5]Department of Pulmonary Medicine, The Third Affiliated Hospital of Yunnan University of Traditional Chinese Medicine, Kunming, Yunnan, People's Republic of China; [6]Department of Pharmacy, Second Affiliated Hospital of Naval Medical University, Shanghai, People's Republic of China

*These authors have contributed equally to this work

Correspondence: Jianguo Sun, Department of Pharmacy, Second Affiliated Hospital of Naval Medical University, No. 415, Fengyang Road, Shanghai, 200003, People's Republic of China, Tel +86-021-81886181, Email 1240603832@stu.cqmu.edu.cn; Danxia Wei, Department of Nephrology and Rheumatology, The Third Affiliated Hospital of Yunnan University of Traditional Chinese Medicine, No. 2628 Xiangyuan Street, Kunming, Yunnan, 650500, People's Republic of China, Tel +86-0871-63125335, Email 15398558606@163.com

Purpose: The in-house preparation Qingre Runzao formula (QRRZF) has been used for decades in our hospital to treat asthma with good efficacy, but its underlying mechanisms and key components remain unclear. This study aims to elucidate the potential mechanisms and key components by which the QRRZF ameliorates asthma.

Methods: UPLC-MS/MS was employed to identify the components of the QRRZF; therapeutic targets were predicted with SwissTargetPrediction and Super-Pred. Asthma transcriptomic data were obtained from GEO and differentially expressed genes were identified (GSE43696 and GSE147878). Venn analysis yielded potential targets of the QRRZF against asthma. GO and KEGG enrichment analyses with Metascape identified key pathways; the pathway-associated proteins served as receptors for molecular docking to rank drug-receptor affinities, thereby identifying key anti-asthma components. CETSA was performed on 16HBE cells cultured in vitro to verify docking results. CCK-8 and ELISA assessed the anti-asthma effects of the key components in vitro, and an HDM-induced asthma mouse model evaluated its efficacy in vivo.

Results: A total of 21 components and 827 predicted targets were obtained; 1250 asthma-related targets were extracted from GEO, yielding 76 potential therapeutic targets. Enrichment analysis suggested calcium signaling pathway as the main pathway; molecular docking showed Deacetyl Ophiopojaponin A (DOA) bound most tightly to Cav2.3, confirmed by CETSA. In vitro experiments demonstrated that DOA protected 16HBE cells from damage induced by house dust mites, reducing the levels of inflammatory cytokines and alleviating airway inflammation, such IL-6, IL-13, and TNF-α. In vivo experiments showed that DOA reduced inflammatory cell infiltration and airway inflammation in the lung bronchioles, protecting the epithelial barrier and demonstrating significant therapeutic efficacy. These results indicate that DOA exerts potent anti-asthma effects by inhibiting the Cav2.3 calcium channel.

Conclusion: This study reveals that calcium signaling pathway is the principal mechanism by which QRRZF improves asthma, and DOA is the key therapeutic component, which alleviates asthma-induced airway inflammation by inhibiting Cav2.3 expression and reducing calcium load in airway epithelial cells.

Keywords: Qingre Runzao formula, asthma, Deacetyl Ophiopojaponin A, CETSA, calcium signaling pathway

Introduction

Bronchial asthma, hereinafter referred to as asthma, is a common chronic inflammatory airway disease characterized by airway hyperresponsiveness and variable airflow limitation.[1] Clinically, it presents with recurrent symptoms such as

https://doi.org/10.2147/JIR.S579513
Received: 13 November 2025
Accepted: 30 April 2026
Published: 16 May 2026

Graphical Abstract

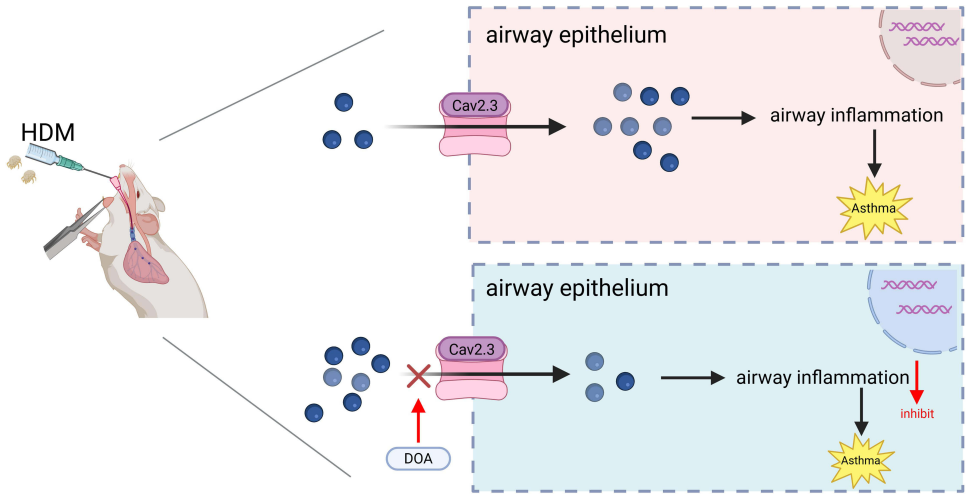

wheezing, shortness of breath, coughing, and chest tightness. The global prevalence of asthma is 3.57%,[2] with an estimated prevalence of 4.2% in China,[3] and the incidence is increasing annually. The main pathological features of asthma-induced airway inflammation and remodeling. The inflammatory cell infiltration and airway wall structural changes are primary obstacles in treating asthma. Currently, the first-line treatment for asthma is low-dose inhale corticosteroids (ICS) combined with long-acting β2-agonists (LABA).[4,5] ICS control airway inflammation, while LABA dilates the bronchi to relieve asthma symptoms, which shows a strong synergistic effect. Notably, in current clinical practice for asthma, physicians are often trapped in a box built around controlling patients' symptoms;[6] therefore, these drugs only target symptoms and do not alter the fundamental characteristics of the disease. Long-term administration may also lead to side effects such as hypokalemia, hypertension, and glucose metabolism disturbances.[7,8] Clinical management of asthma and asthma-induced airway inflammation still faces formidable challenges, driving a growing number of patients to seek alternative therapies such as Traditional Chinese Medicine, acupuncture, and ethnomedicine, etc.

Qingre Runzao formula (QRRZF) is an effective prescription used for over 30 years in treating asthma by renowned Yunnan-based traditional Chinese medicine practitioner Lu Jialong. Professor Lu believes that the primary pathogenesis of asthma is the internal retention of phlegm-dampness, triggered by external pathogenic factors.[9] In QRRZF, mulberry leaves, with their uplifting and cooling nature, serve as the chief ingredient to dispel lung dryness and wind-warm pathogens. Bitter apricot kernels work as the secondary ingredient, working synergistically with mulberry leaves to regulate lung *qi*. Ladybell root and dwarf lilyturf root tuber moisturize the lungs and stomach to boost fluid production, while reed rhizome promotes diuresis and *qi* transformation. The QRRZF simultaneously nourishes and facilitates fluid metabolism, ensuring proper fluid distribution and phlegm elimination. Preliminary clinical studies have shown that QRRZF effectively alleviates dry cough in patients.[10] Our further research has confirmed that QRRZF prolongs the latency period of asthma in mice, reduces leukocyte count, decreases mucus secretion in the airways, lowers MUC5AC secretion, and modulates the imbalance of Treg/Th17 cells to alleviate asthma.[11] Its mechanisms may be associated with the regulation of IL-13, IL-10, and IL-17A levels in bronchoalveolar lavage fluid, as well as serum IgE and Ovalbumin-IgE levels.[12,13] However, the key components and mechanisms of the QRRZF against asthma remain unclear.

Relying solely on data mining from databases like TCMSP can lead to a skewed assessment of the pharmacological relevance of active components. This often results in overly homogenized results in network pharmacology analysis, where ubiquitous components such as quercetin, kaempferol, and β-sitosterol are recurrently identified as "panaceas" for various diseases.[14] Therefore, in this study, UPLC-Q/TOF-MS/MS was used to identify the components of QRRZF, and network pharmacology combined with GEO data mining was employed to reveal the core targets and mechanisms of

QRRZF against asthma. Molecular docking was performed with core targets as receptors to obtain key components of QRRZF, and CETSA was used to verify the binding between the key components and core targets. Finally, the anti-asthma potential of the key components was evaluated both in vitro and in vivo. This study integrates multiple approaches to identify the key components and mechanisms of the QRRZF against asthma, providing valuable data for its further research and clinical application.

Materials and Methods

Reagents

Qingre Runzao formula (Batch No.: SZYY24091503) was prepared by the Department of Pharmacy, Third Affiliated Hospital of Yunnan University of Chinese Medicine (Lot: KMSZ-241014), and quality control of QRRZ was conducted according to our previous studies (1 mL QRRZ contains 3.94 g crude drugs).[13] Deacetyl ophiopojaponin A (DOA) standard (Batch No.: MUST-24110709, purity > 98%) was purchased from Chengdu MUST Bio-technology Co., Ltd. House dust mites (D. pteronyssinus, HDM) (Lot: XPB82D3A2.5) were obtained from Greer Labs (North Carolina, America). Fetal bovine serum (Batch No.: A5256701) was purchased from Gibco (USA). KM (Batch No.: #2101) was purchased from ScienCell Research Laboratories (USA). 12% SDS-PAGE precast gels (Batch Nos.: P0056B), RIPA lysis buffer (Batch Nos.: P0013B), primary antibody dilution solution (Batch Nos.: P0023A), CCK-8 kit (Batch Nos.: C0038), BCA protein assay kit (Batch Nos.: P0012S), and HRP-labeled secondary antibody (Batch Nos.: A0208) were purchased from Shanghai Beyotime Biotechnology Co., Ltd. The ELISA kits (IL-6: Batch No.: LK-EK106, IL-13: Batch No.: LK-EK113, TNF-α: Batch No.: LK-EK182) were obtained from MultiSciences Biotech Co., Ltd. The Cav2.3 rabbit polyclonal antibody (Batch No.: ab230640) and GAPDH antibody (Batch No.: ab128915) were purchased from Abcam.

UPLC-Q/TOF-MS Analysis

Sample Preparation: 100μL of QRRZF was mixed with 200μL of methanol, vortexed for 3 minutes, and then centrifuged at 3000 rpm for 10 minutes at 4°C. The supernatant was collected and filtered using a 0.22μm filter membrane. The filtered sample was then transferred to an autosampler vial for analysis. The instruments used included the X500B Q/TOF system from AB SCIEX and ACQUITY UPLC I-Class system from Waters. The mass spectrometry data were processed using SCIEX OS software. A drug component database was constructed by reviewing literature and chemical databases. The collected mass spectrometry data were then compared with the database constructed to identify the components.

Chromatographic conditions: The chromatographic column used was ACQUITY UPLC® HSS T3 (2.1×100 mm, 1.8 μm). The mobile phase consisted of A: acetonitrile and B: 0.1% formic acid in water. The gradient elution program was as follows: 0–2 min, 5% A; 2–10 min, 5% A → 12% A; 10–25 min, 12% A → 25% A; 25–35 min, 25% A → 40% A; 35–40 min, 40% A → 60% A; 40–45 min, 60% A → 90% A; 45–50 min, 90% A → 95% A; Post-run: 50–52 min, 95% A → 5% A. The column temperature was set at 30°C, the injection volume was 5μL, and the flow rate was 0.3 mL/min.

Mass spectrometry conditions: The ion source used was an Electrospray Ionization (ESI) source, performing both positive and negative ion scanning. The ion source temperature was set to 280°C, and the nebulizer temperature was 350°C. The curtain gas pressure was 35 psi. The spray voltage was 5 kV (positive ion mode) and −4 kV (negative ion mode). The declustering potential was 70 V. The full scan range was m/z 80~1500.

Identification of Potential Targets

Chemical structures of drug components were downloaded from PubChem and imported into SwissTargetPrediction and Super-Pred to predict relevant targets. Transcriptomic data associated with asthma were then collected from GEO, including GSE43696 and GSE147878. The GSE43696 dataset comprises 20 normal bronchial epithelial cell samples and 88 bronchial epithelial cell samples from asthma patients. The GSE147878 dataset comprises 13 normal endobronchial biopsy samples and 60 endobronchial biopsy samples from asthma patients. After annotating the data, differentially expressed genes were identified using the Limma program. For the GSE43696 dataset, the screening criteria for differential expression were $|\text{fold change}| \geq 1.5$, $P \leq 0.05$, and $FDR \leq 0.05$. For the GSE147878 dataset, the screening

criteria were |fold change| ≥ 1.3, P ≤ 0.05, and FDR ≤ 0.05. All targets were standardized in the Uniport database, and Venn analysis identified potential targets of QRRZF ameliorates asthma.

GO and KEGG Enrichment Analyses

GO and KEGG enrichment analysis can quickly elucidate the mechanisms associated with the identified targets. Potential targets were imported into the MetaScape for GO and KEGG enrichment analysis, using Homo sapiens as the analysis species and $P < 0.05$ as the screening criterion. The results were ranked by *P*-value and visualized using the ggplot2 package.

Molecular Docking

The above results suggest that QRRZF may exert its effects through the calcium ion signaling pathway. Therefore, we selected calcium ion channel proteins as receptors and downloaded protein structure files from the PDB, including N-, R-, P/O-, and L-type calcium ion channels (PDB IDs: 7MIX, 7XLQ, 8FOA, and 8WE6). The proteins were preprocessed using PyMol to remove water molecules and add hydrogen atoms. The CASTp 3.0 was used to identify the binding pockets for molecular docking. The chemical structures of the QRRZF components were downloaded from PubChem, and molecular docking was performed using AutoDock 1.5.7 with default parameters. The docking results were ranked by binding energy and visualized using a heatmap. A lower binding energy indicates a tighter binding between the compound and the protein. Finally, the top three compounds with the lowest binding energy were visualized for their binding conformations using PyMOL.

Cell Culture

Complete culture medium was prepared by supplementing KM with 10% fetal bovine serum and 1% penicillin-streptomycin. 16HBE cells were seeded in the complete medium and incubated in a humidified cell culture incubator at 37°C with 5% CO2. When the cells reached 80% confluence, they were passaged. Based on previous studies, the asthma cell model was established using the house dust mite (HDM) method. Specifically, when the cells reached 60% confluence, they were treated with 10μg/mL HDM for 12 hours to establish cell model of asthma-induced airway inflammation.

Western Blotting

Proteins were extracted from cells and tissues using RIPA buffer containing PMSF. The proteins were loaded onto a 12% SDS-PAGE gel for electrophoretic separation, with the following voltage conditions: 80V for 30 minutes and 120V for 1 hour. After electrophoresis, the proteins were transferred to a PVDF membrane at 0.4 mA for 5 hours. Following transfer, the membrane was blocked using a rapid blocking solution without protein, then incubated overnight at 4°C with the primary antibody (diluted 1:2000). After incubation, the membrane was washed three times with TBST, followed by incubation with the secondary antibody (diluted 1:1000) at room temperature for 2 hours. The membrane was washed again with TBST three times and then detected using ECL reagent for chemiluminescence. The images were captured using gel imaging system. Finally, the protein band density was quantified using ImageJ, with GAPDH as the internal control for calculating the relative expression of the target protein.

CETSA Assay

Human bronchial epithelial cells (16HBE cells) (Batch No.: ARIS241205) were purchased from ORiCells Biotechnology (Shanghai) Co., Ltd. The cells in the logarithmic growth phase were seeded into T75 culture flasks. Once the cells reached confluence, they were collected and lysed on ice using RIPA buffer to obtain cell lysates. The lysates were evenly divided into two portions. One portion was incubated with the drug for 30 minutes, and the other was treated with DMSO. After incubation, both portions were further divided into six aliquots and centrifuged at 17,400 g for 10 minutes to collect the supernatant. The supernatants were then treated at 38, 44, 50, 56, 62, and 69°C for 10 minutes, followed by the addition of protein loading buffer. Western blotting was used to detect the expression levels of the target protein. The results were analyzed using the Boltzmann sigmoidal function in GraphPad Prism.

CCK-8 Assay

16HBE cells in the logarithmic growth phase were seeded at a density of approximately 5×10^3 cells/well in a 96-well plate. The cells were divided into the control, model, and treatment groups. All groups, except for the control group, were treated with 10μg/mL HDM. After 12 hours of incubation, the treatment group was exposed to different concentrations of DOA (5μM, 10μM, 20μM, 40μM, 80μM, and 160μM). After 24 hours, 10 μL of CCK-8 reagent was added to each well and incubated for 2 hours. The absorbance at 450 nm was measured using a microplate reader, and the results were calculated.

ELISA

16HBE cells in the logarithmic growth phase were seeded at a density of approximately 2×10^4 cells/well in a 6-well plate. Cells were divided into control group, model group, DOA treatment group, and positive control group. All groups except the control group were stimulated with 10 μg /mL HDM, and then treated with 20 μM or 40 μM DOA. In the positive control group, 40 μM DXM was administered in place of DOA. After 24 hours of drug treatment, the cell culture supernatants were collected. The levels of TNF-α, IL-6, and IL-13 in the supernatants were measured according to the manufacturer's instructions. The results were analyzed and visualized using GraphPad Prism software.

Ca^{2+} Microfluorimetry

The level of Ca^{2+} in 16HBE cells was detected using fluorescent indicator Fluo-4AM (Fluo-4, Thermo Fisher Scientific). First, mix Fluo-4 AM/DMSO solution with 20% Pluronic F127 solution at 1:1 ratio; dilute with HBSS buffer to obtain 5 μM working solution; incubate working solution with cells in 37 °C incubator for 20 min; then add 5 volumes HBSS buffer containing 1% FBS, and continue incubation for 40 min to complete dye loading. After staining, wash cells 3 times with HEPES buffer saline, then resuspend cells in HEPES buffer saline and adjust cell density to 1×10^5 cells/mL. Equilibrate cell suspension at 37 °C for 10 min, then detect cellular Ca^{2+} level by flow cytometry; set fluorescence detection parameters to excitation wavelength 506 nm, emission wavelength 526 nm.

Cav2.3 Overexpression Plasmid Construction and Cell Transfection

Using human total cDNA as template, the target gene fragment was amplified with gene-specific primers: Cav2.3-F: CCTCAGGATGGCTCGCTTC; Cav2.3-R: GAGCAGCCTCTAGCATTTGTCA. Then high-fidelity PCR was performed with vector-homology primers: upstream primer (Cav2.3-HF): CAAGTTAACAACAAGGATCCATGGCTCGCTTCGGGGA; downstream primer (Cav2.3-HR): CTAAATCCAGTGACCTCGCTAGCATTTGTCATCTTCTTCCGTGTC. The pHBAAV-CMV vector was double-digested with BamHI and XhoI (NEB), and the linearized vector was recombined with the gene fragment by In-Fusion cloning. The recombination product was added to DH5α competent cells, positive colonies were selected with ampicillin, and plasmid correctness was verified by Sanger sequencing. For cellular Cav2.3 over-expression, the plasmid was transfected into cells with Lipo3000; for in vivo over-expression, the plasmid was packaged into AAV, and Cav2.3 AAV was delivered by tail-vein injection. Finally, Western blot was used to confirm Cav2.3 overexpression efficiency.

Animal Experiment Procedures and Treatment

Five-week-old BALB/c mice, weighing 20 ± 2 g, were purchased from Shanghai Yishang Biotechnology Co., Ltd. [License No.: SCXK (Hu) - 2022-0011]. All animals were housed in a constant temperature environment at 24°C with a 12-hour light/dark cycle and free access to food and water. The study was conducted in strict accordance with ARRIVE 2.0 guidelines to ensure the ethical use of animal research. The animal experiments were approved by the Animal Ethics Committee of Yunnan University of Chinese Medicine [Ethics No.: R-062022G105].

A total of 30 BALB/c mice were divided into the control group, model group, high- and low-dose DOA groups, and the positive control group (n=6). Except for the CTL mice, all animals received a single tracheal injection of 3 μg HDM on day 1. From day 7 onward, they were challenged intranasally with 10 μg HDM once daily for five consecutive days. After successful modeling, the high- and low-dose DOA groups received 20 mg/kg/d and 10 mg/kg/d of DOA treatment, respectively, and dexamethasone (DXM) at 1.56 mg/kg/day. All drugs were administered via intraperitoneal injection. The BALF was collected after the airway hyperresponsiveness assessment, then the mice were euthanized with deep isoflurane (5%) anesthesia, and the lung bronchial tissue was harvested.

Airway Hyper-Responsiveness Assessment

Airway hyper-reactivity was measured without invasion using whole-body plethysmography, with enhanced pause (Penh) as the readout. Conscious mice were positioned in a WBP-4M chamber (TOW-INT, China) and exposed for 60s to nebulized methacholine at stepwise concentrations of 3.25, 7.5, 15, and 30 mg mL^{-1}. Penh was recorded every 10s during the 5 min that followed each exposure; the mean of the final 30 recordings was assigned as the response for that concentration.

Bronchoalveolar Lavage Fluid (BALF) Collection and Analysis

Following the last dose, the chest was accessed through an abdominal approach. With the right bronchus occluded, a V-cut was made in the main bronchus; 0.3 mL ice-cold PBS was gently infused into the left lung via a syringe and withdrawn three times. Fluid recovering ≥70% was accepted as bronchoalveolar lavage fluid (BALF), centrifuged (4 °C, 2000 rpm, 5 min), split into aliquots and kept at –80 °C. A 10 μL aliquot of the cell suspension was taken from the pellet and subjected to cell counting under an inverted microscope to determine the total cell count. In addition, a 20 μL aliquot of the cell suspension was stained according to the Wright-Giemsa staining instructions to count the numbers of lymphocytes, neutrophils, and eosinophils in the BALF.

Histopathological Examination and Immunohistochemical Staining

Lung bronchial tissues from mice were collected for histopathological examination. The tissues were first embedded in paraffin and sectioned into 5μm slices. H&E, Masson, and PAS staining were performed on the tissue sections. In addition, immunohistochemical staining was used to detect the expression of ZO-1 in the bronchi. All pathological examinations and staining procedures were outsourced to Shanghai Ruiyu Biotechnology Co., Ltd.

Statistical Analysis

All statistical analyses were performed using GraphPad Prism. Comparisons between two groups were made using the *t*-test, while comparisons among multiple groups were performed using one-way ANOVA. Results are presented as Mean ± SEM, and $p < 0.05$ was considered statistically significant.

Results

Chemical Component Identification and Target Prediction of QRRZF

The chemical components of QRRZF were analyzed using UPLC-Q/TOF-MS (Figure 1). From the total ion chromatogram, 21 components of QRRZF were identified (Table 1). The chemical structures of these 21 components were obtained from the PubChem, and these components were then imported into databases such as Super-Pred and SwissTargetPrediction. A total of 827 targets for QRRZF were predicted.

Identification of Potential Targets of QRRZF in Alleviating Asthma

Asthma-related transcriptomic data were obtained from GEO. Differential analysis was performed to identify differentially expressed genes in asthma, including GSE43696 (Figure 2A) and GSE147878 (Figure 2B). After merging these differentially expressed genes, a total of 1250 asthma-related targets were identified. Venn analysis was then conducted between the targets of QRRZF and the 1250 asthma-related targets, resulting in 76 intersecting targets (Figure 2C), and Figure 2D depicts the interplay among the 76 targets. Results show that these 76 targets represent the potential therapeutic targets of QRRZF against asthma.

GO and KEGG Enrichment Analysis of Potential Targets

GO and KEGG enrichment analysis of the potential targets was performed using Metascape. The GO enrichment analysis indicated that these potential targets are mainly associated with biological processes such as protein phosphorylation, MAPK cascade regulation, and protein kinase activity (Figure 3A). The KEGG enrichment analysis revealed that QRRZF primarily alleviates asthma by modulating the calcium ion signaling pathway (Figure 3B).

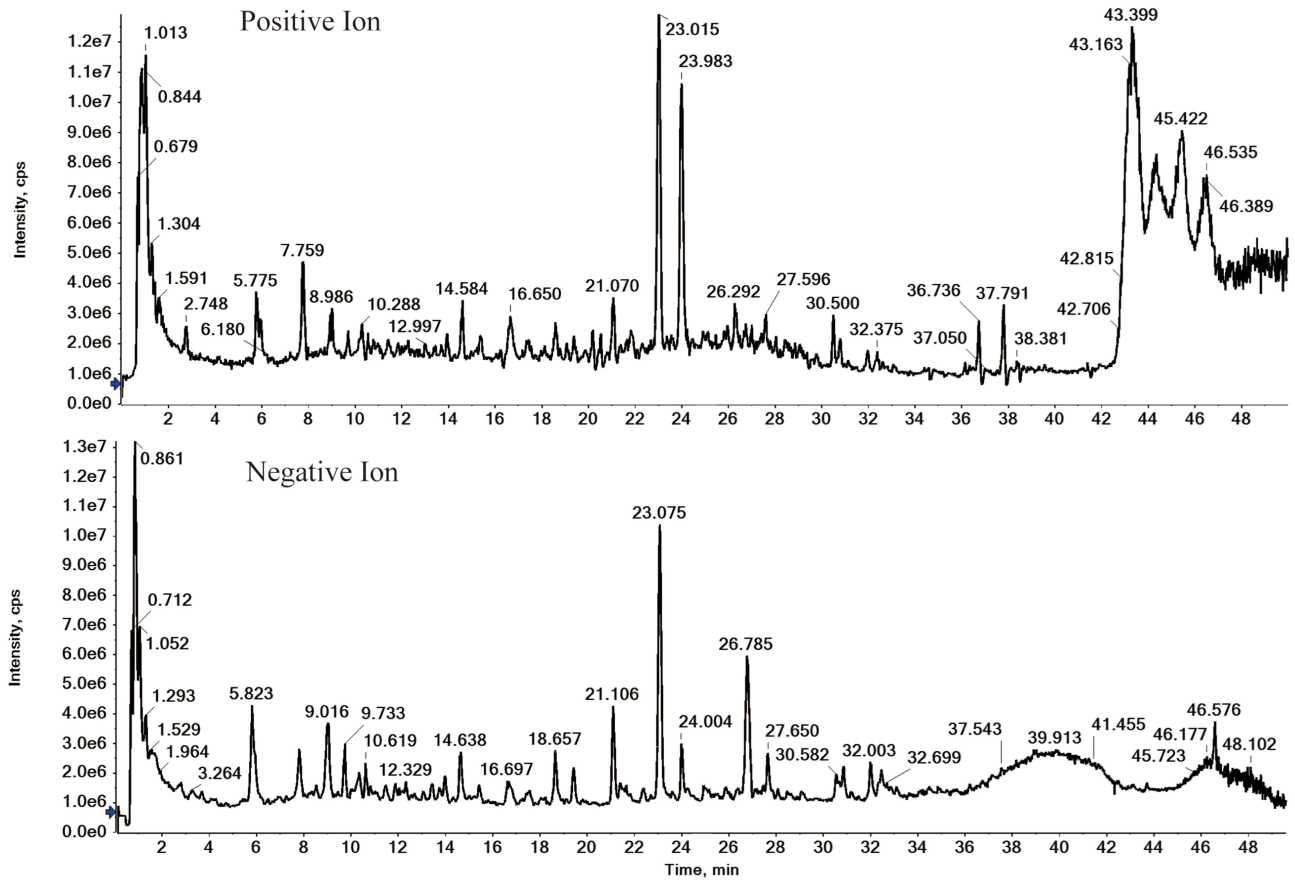

Figure 1 Total ion chromatogram of QRRZF under positive and negative ion modes by UPLC-MS/MS.

DOA is the Key Component of QRRZF in Alleviating Asthma

In summary, QRRZF may alleviate asthma by modulating the calcium ion signaling pathway. Common calcium ion channel proteins include L-type, N-type, and R-type channels. Therefore, in this study, four types of calcium ion channel proteins were selected from the PDB as receptors, and 21 components of QRRZF were used as ligands for molecular

Table 1 The Identification Components of QRRZF by UPLC-MS/MS Analysis

Peak No.	RT (min)	Compound	Formula	Calculated (Da)	Selected Ion	Mass Accuracy (ppm)	MS/MS
1	0.86	Quinic acid	$C_7H_{12}O_6$	191.0560	$[M-H]^-$	2.09	173.0462/109.0289/93.0344
2	1.65	Guanosine	$C_{10}H_{13}N_5O_5$	284.1004	$[M+H]^+$	3.17	152.0563/135.0302
3	2.76	Phenylalanine	$C_9H_{11}NO_2$	166.0869	$[M+H]^+$	0.60	120.0809/103.0543/77.0386
4	5.93	Neochlorogenic acid	$C_{16}H_{18}O_9$	353.0873	$[M-H]^-$	0.00	191.0561/179.0349/135.0453
5	5.95	Tryptophan	$C_{11}H_{12}N_2O_2$	203.0825	$[M-H]^-$	1.97	142.0661/116.0506/74.0247
6	9.06	Chlorogenic acid	$C_{16}H_{18}O_9$	353.0873	$[M-H]^-$	0.00	191.0562
7	9.75	Cryptochlorogenic acid	$C_{16}H_{18}O_9$	353.0875	$[M-H]^-$	0.57	191.0563/173.0454/135.0451
8	13.83	p-Coumaric acid	$C_9H_8O_3$	163.04	$[M-H]^-$	3.07	119.0503/93.0346
9	15.93	Ferulic acid	$C_{10}H_{10}O_4$	193.0501	$[M-H]^-$	0.00	178.0270/134.0375
10	18.65	Rutin	$C_{27}H_{30}O_{16}$	609.1455	$[M-H]^-$	−0.16	300.0270/271.0244/255.0296
11	19.44	Isoquercitrin	$C_{21}H_{20}O_{12}$	463.0878	$[M-H]^-$	0.22	300.0277/271.0249/255.0304
12	21.11	Naringin	$C_{27}H_{32}O_{14}$	579.1717	$[M-H]^-$	0.52	271.0616/151.0039
13	21.69	Kaempferol-3-O-rutinoside	$C_{27}H_{30}O_{15}$	593.1507	$[M-H]^-$	0.00	285.0404/255.0295
14	22.38	Astragalin	$C_{21}H_{20}O_{11}$	447.0931	$[M-H]^-$	0.67	285.0405/255.0300/227.0351

(*Continued*)

https://doi.org/10.2147/JIR.S579513

Table 1 (Continued).

Peak No.	RT (min)	Compound	Formula	Calculated (Da)	Selected Ion	Mass Accuracy (ppm)	MS/MS
15	22.95	Peimine	$C_{27}H_{45}NO_3$	432.3483	$[M+H]^+$	1.39	414.3349/398.3044
16	23.02	Hesperidin	$C_{28}H_{34}O_{15}$	609.1817	$[M-H]^-$	−0.49	325.0720/301.0712/286.0484
17	24.04	Peiminine	$C_{27}H_{43}NO_3$	430.3336	$[M+H]^+$	3.49	412.3198/396.2895
18	36.73	Nobiletin	$C_{21}H_{22}O_8$	403.1401	$[M+H]^+$	1.98	388.1148/373.0906
19	38.43	Tangeretin	$C_{20}H_{20}O_7$	373.1292	$[M+H]^+$	1.34	358.1043/343.0807
20	39.68	Ophiopogonin D	$C_{44}H_{70}O_{16}$	899.4609	$[M+HCOO]^-$	−3.56	853.4574/721.4165/575.3542
21	38.86	Deacetyl ophiopogonin A	$C_{46}H_{72}O_{18}$	957.4691	$[M+HCOO]^-$	−0.52	911.4617/869.4502/737.4117

docking. The results showed that these components generally exhibited higher binding energy with R-type calcium channel protein Cav2.3 (PDB ID: 7XLQ) than with other calcium ion proteins. Among them, DOA showed the strongest binding to Cav2.3, with a binding energy of −11.6 kcal/mol (Figure 4A). PyMOL was then used to visualize the binding conformation of DOA with Cav2.3, showing that DOA mainly binds to Cav2.3 through the ALA-324 and ARG-1642 sites (Figure 4B). These results suggest that QRRZF exerts its therapeutic effects on asthma primarily by regulating Cav2.3, with DOA being the key active component.

CETSA is a common method to detect the binding of small molecules to proteins. Therefore, we further examined the binding of DOA to Cav2.3 using CETSA. The results showed that DOA treatment increased the thermal stability of Cav2.3, inhibited its degradation, and caused a rightward shift in the protein denaturation curve (Figure 4C and D). This indicates that DOA can tightly bind to Cav2.3.

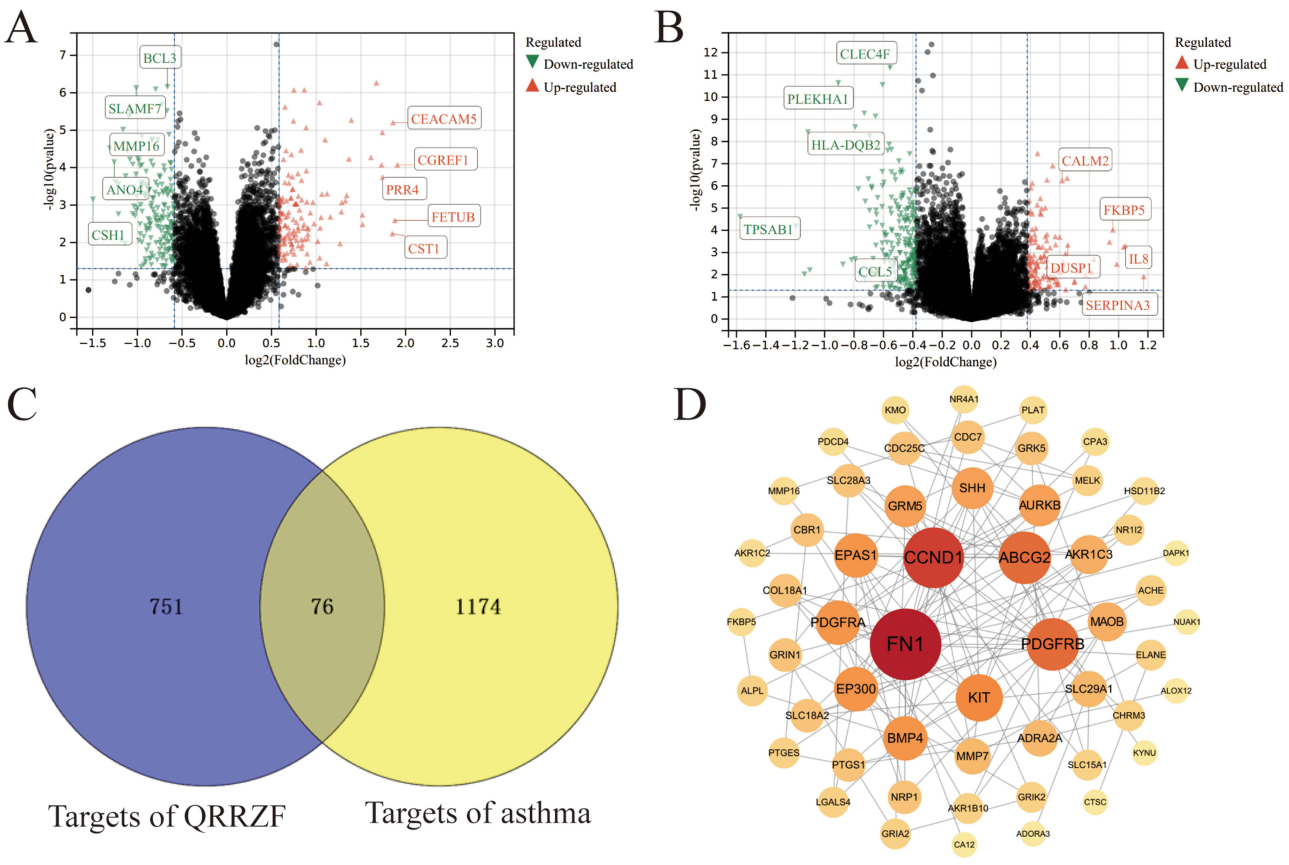

Figure 2 Screening of potential therapeutic targets of QRRZF for asthma. (**A** and **B**): Volcano plots of differential expression in datasets GSE43696 and GSE147878; red indicates up-regulated genes and green indicates down-regulated genes; (**C**) Venn analysis identified 76 potential targets through which QRRZF may ameliorate asthma; (**D**) Protein–protein interaction network of the 76 potential targets, As the Degree value decreases, the colors descend from red to yellow and circles shrink.

https://doi.org/10.2147/JIR.S579513

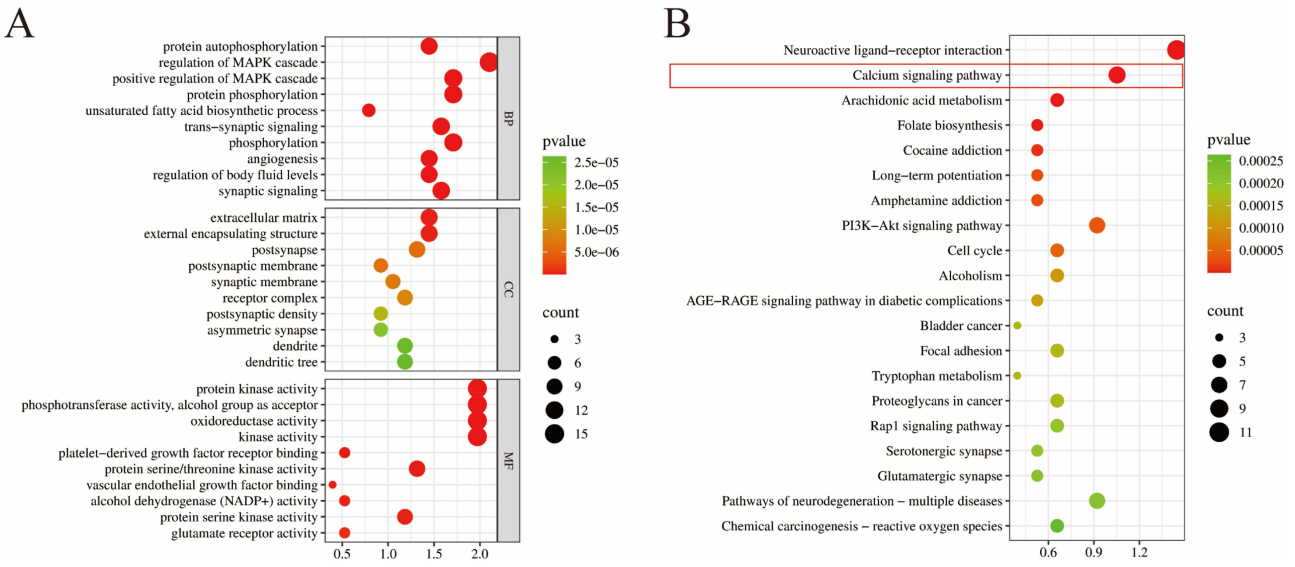

Figure 3 GO (**A**) and KEGG (**B**) enrichment analyses of potential targets.

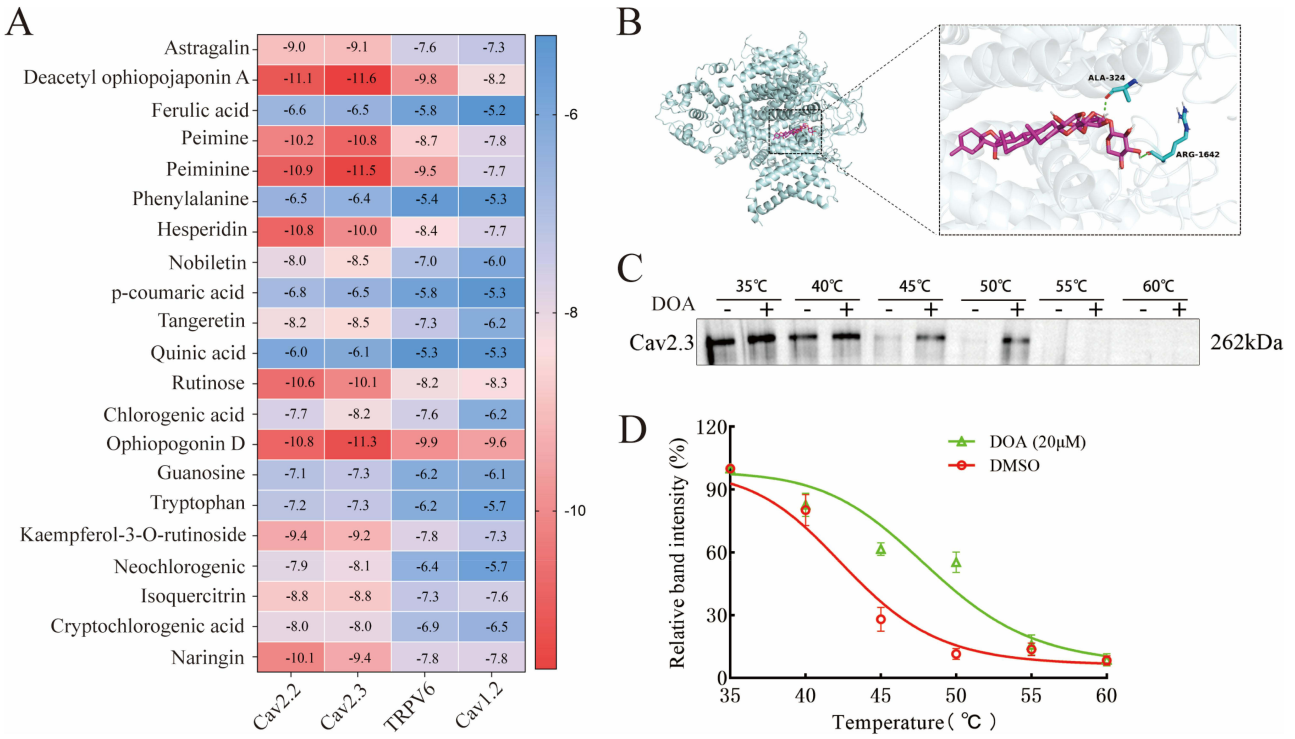

Figure 4 Molecular docking to identify key components of QRRZF in alleviating asthma. (**A**) Binding energies of 21 QRRZF components docked to the four calcium-channel proteins; As the binding energy increases, the color-coded from red to blue; (**B**) 3D binding pose of DOA within the Cav2.3 protein; (**C** and **D**) CETSA assay confirming the tight interaction between DOA and Cav2.3 (n=3).

DOA Inhibits Cav2.3 and Reduces Intracellular Ca^{2+} Levels to Ameliorate Asthma in vitro

An asthma cell model was established in vitro using HDM-treated 16HBE human bronchial epithelial cells, followed by treatment with DOA to evaluate its effect on alleviating asthma. The results showed that HDM significantly inhibited the proliferation of 16HBE cells, while DOA significantly promoted cell proliferation (Figure 5A). Then, Fluo-4 AM was

https://doi.org/10.2147/JIR.S579513

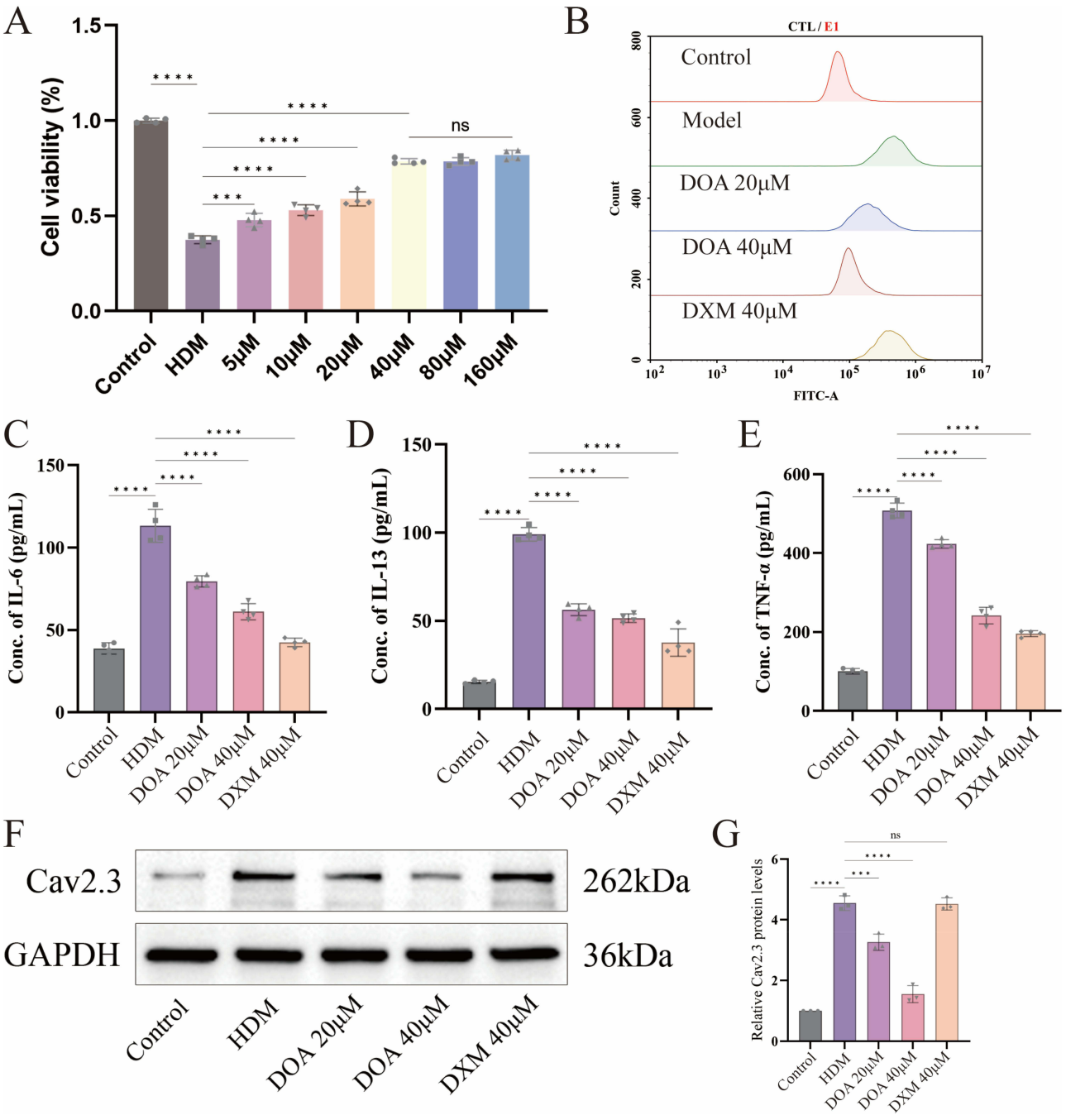

Figure 5 DOA alleviates asthma by suppressing Cav2.3 expression and lowering intracellular Ca^{2+} in 16HBE cells. (**A**) CCK-8 assay for DOA effect on HDM-stimulated 16HBE proliferation (n = 3); (**B**) Flow-cytometric quantification of intracellular Ca^{2+} after DOA treatment (n = 3); (**C**–**E**) ELISA measurement of DOA-induced reduction in IL-6, IL-13 and TNF-α levels in 16HBE cells; (**F** and **G**) Western blot detects Cav2.3 expression after DOA treatment (n = 3). All data are presented as Mean ± SEM; compared with the Model group: * $P < 0.05$; ** $P < 0.01$; *** $P < 0.001$; **** $P < 0.0001$.

used to monitor intracellular Ca^{2+} in 16HBE cells. The results showed that compared with the control, HDM challenge produced a marked rise in Fluo-4 fluorescence, indicating Ca^{2+} overload. DOA treatment lowered the intracellular Ca^{2+} signal, demonstrating that DOA can alleviate HDM-induced Ca^{2+} overload (Figure 5B). ELISA results indicated that HDM significantly upregulated the levels of IL-6, IL-13, and TNF-α, whereas DOA significantly inhibited these levels and relieved airway inflammation in asthma (Figure 5C–Figure 5E). Finally, Western blot was used to evaluate the effect of DOA on Cav2.3 expression. The results showed that DOA treatment markedly reduced Cav2.3 levels in 16HBE cells (Figure 5F and Figure 5G).

To further demonstrate the pivotal role of Cav2.3 in DOA-mediated amelioration of asthma, we next evaluated the impact of Cav2.3 overexpression in 16HBE cells on the efficacy of DOA (Figure 6A and B). The results showed that overexpressing Cav2.3 significantly enhanced the inhibitory effect of DOA on Cav2.3 expression (Figure 6C and D). Flow-cytometric analysis further revealed that, compared with the DOA-only group, Cav2.3 overexpression elevated intracellular Ca^{2+} levels (Figure 6E). Additionally, CCK-8 assays showed that Cav2.3 overexpression reversed the protective effect of DOA on HDM-stimulated 16HBE cells (Figure 6F), and ELISA results indicated that, compared with DOA treatment alone, Cav2.3 overexpression exacerbated airway inflammation (Figure 6G–I). Overall, these findings indicate that DOA possesses promising therapeutic potential against asthma by alleviating airway inflammation via suppression of Cav2.3 expression and is a promising candidate for asthma therapy.

DOA Exhibits Strong Anti-Asthma Effects in vivo

The therapeutic effect of DOA was further evaluated in an asthma mouse model, and Figure 7A illustrates the workflow of the animal experiment. The results showed that DOA treatment significantly attenuated airway hyperresponsiveness in asthma mice (Figure 7B). ELISA results show that DOA can reduce the levels of Ig-E, IL-6, IL-13, and TNF-α in BALF (Figure 7C–F). Additionally, analysis of cell counts in BALF revealed that DOA treatment significantly reduced the total cell count, as well as the numbers of lymphocytes, neutrophils, and eosinophils in BALF (Figure 7G–J). H&E staining results showed that, compared to the control group, the model group exhibited extensive inflammatory cell infiltration

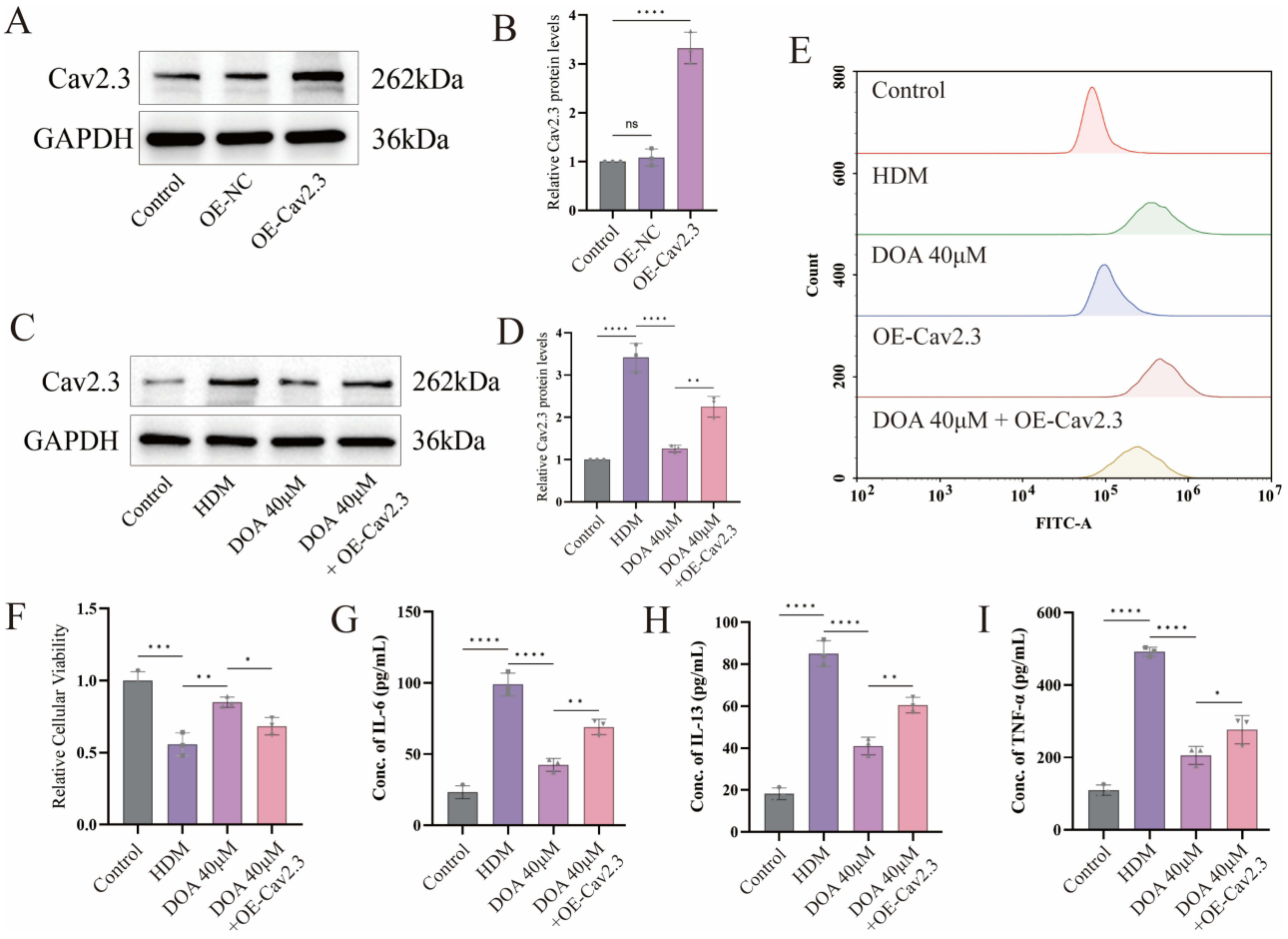

Figure 6 Cav2.3 overexpression reverses the anti-asthma efficacy of DOA. (**A** and **B**) Western blot verification of Cav2.3 overexpression efficiency (n = 3); (**C** and **D**) Western blot showing that Cav2.3 overexpression enhances DOA-mediated suppression of Cav2.3 (n = 3); (**E**) The DOA-induced reduction in intracellular Ca^{2+} is abolished when Cav2.3 is overexpressed (n = 3); (**F**) CCK-8 assay of cell proliferation after Cav2.3 overexpression (n = 3); (**G–I**) Impact of Cav2.3 overexpression on inflammatory cytokines IL-6, IL-13 and TNF-α levels in 16HBE cells (n = 3). All data are presented as Mean ± SEM; compared with the Model group: * $P < 0.05$; ** $P < 0.01$; *** $P < 0.001$; **** $P < 0.0001$.

https://doi.org/10.2147/JIR.S579513

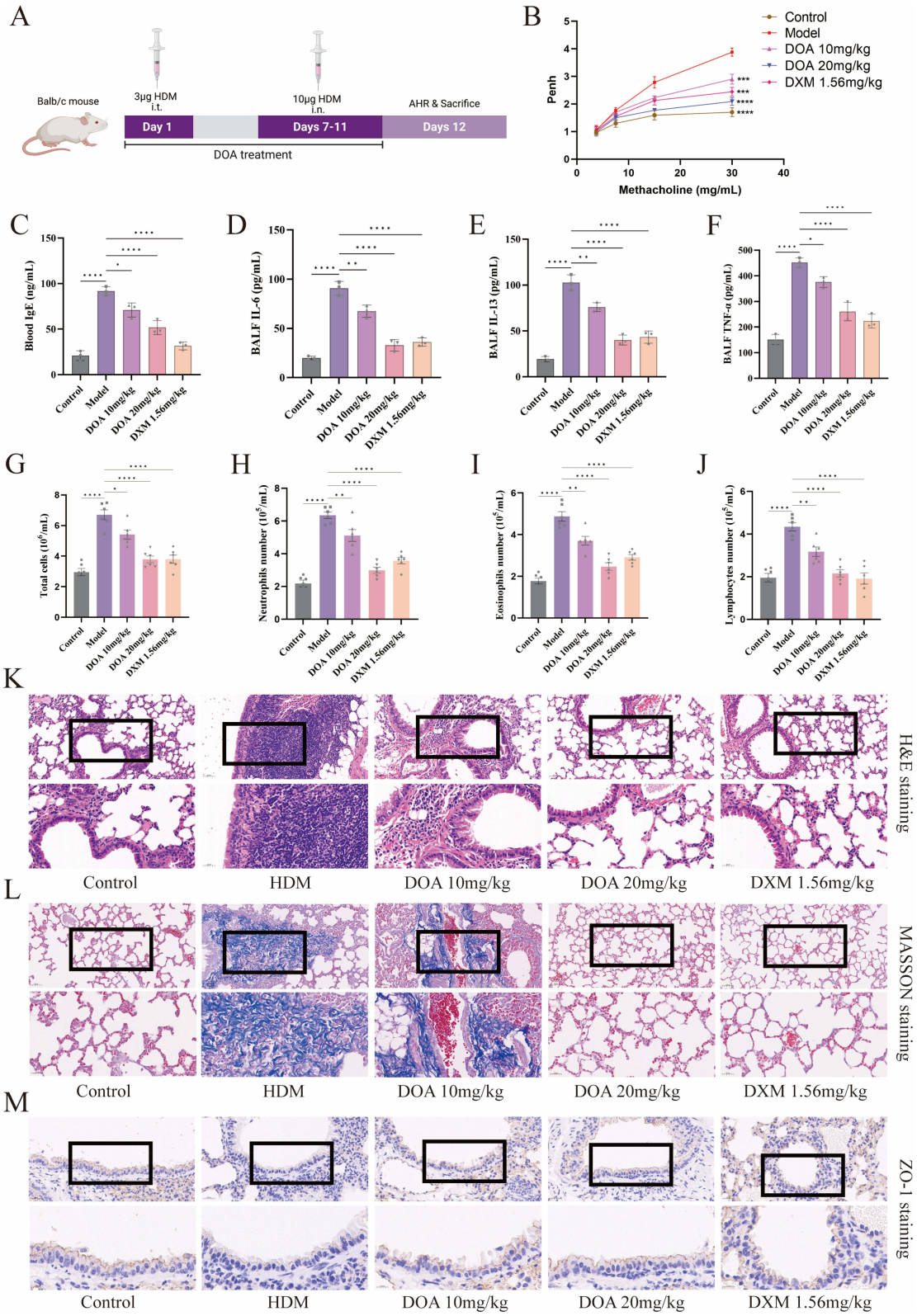

Figure 7 DOA alleviates asthma pathological symptoms. (**A**) Schematic diagram of the animal experiment; (**B**) Pulmonary function assessment (n=6); (**C**) ELISA detection of IgE in serum (n=3); (**D–F**) ELISA detection of IL-6, IL-13 and TNF-α in BALF (n=3); (**G–J**) Cellular analysis in BALF, including total cells, neutrophils, eosinophils, and lymphocytes (n=6); (**K**) H&E staining of bronchioles (n=3); (**L**) Masson staining of bronchioles (n=3); (**M**) ZO-1 expression levels in bronchioles (n=3). All data are presented as Mean ± SEM; compared with the Model group: * $P < 0.05$; ** $P < 0.01$; *** $P < 0.001$; **** $P < 0.0001$.

https://doi.org/10.2147/JIR.S579513

around the alveolar septa and bronchioles, while the DOA-treated group showed a significant reduction in lung lesions (Figure 7K). Masson staining revealed that the alveolar septa in the model group were thickened, with widespread fibrosis around the alveolar septa and bronchioles. In contrast, the DOA-treated group exhibited reduced alveolar septal thickness and significantly alleviated fibrosis and lung damage (Figure 7L). Finally, immunohistochemical staining for ZO-1 was used to assess the therapeutic effects of DOA on bronchial epithelial barrier damage. The results showed that, in the model group, bronchial epithelial cells were loosely arranged with decreased ZO-1 signals at the apical sites of epithelial cells. In the DOA-treated group, the bronchial epithelial cells were tightly arranged, with continuous, dotted positive signals at the cell junctions (Figure 7M). These results confirm that DOA can alleviate asthma-induced airway inflammation in vivo and has a promising anti-asthma potential.

Discussion

Asthma is a common chronic inflammatory airway disease with recurrent and difficult-to-cure symptoms, severely affecting the quality of life of patients.[15] TCM offers significant advantages in treating asthma due to its multi-level, multi-target, and systematic regulation, along with relatively low toxicity and side effects.[16] QRRZF is an effective prescription for treating asthma over 30 years developed by renowned TCM practitioner Lu Jialong, and was improved into an in-house preparation at Kunming Municipal Hospital of Traditional Chinese Medicine. Extensive clinical practice has confirmed the formula's good efficacy in alleviating asthma. Additionally, our previous studies have confirmed the anti-asthma effects of the QRRZF in a mouse model, though its therapeutic components and molecular mechanisms remain unclear. In this study, UPLC-Q/TOF-MS was used to identify the chemical components of QRRZF. Network pharmacology, molecular docking, CETSA, and in vitro experiments were employed to elucidate the molecular mechanisms by which QRRZF alleviates asthma. The results indicate that the QRRZF alleviates asthma by inhibiting the calcium ion signaling pathway, and DOA is the key component of the QRRZF. DOA exerts its effects by targeting and binding to R-type calcium channel protein Cav2.3, thereby inhibiting airway inflammation and relieving asthma. Notably, according to a document from the European Academy of Allergy and Clinical Immunology (EAACI), allergic asthma resulting from airway epithelial barrier damage is classified as type V hypersensitivity. This type is characterized by impaired epithelial barrier function, which promotes immune system activation and subsequently leads to chronic inflammation. Additionally, chemical-mediated type VII hypersensitivity may also be one of the mechanisms of this study.[17] The mechanisms by which DOA improves HDM-induced allergic asthma remain to be further elucidated in future studies.

Numerous studies have shown that calcium ion channels play a crucial role in asthma. Calcium channel blockers can significantly reduce cough, airway obstruction, and airway remodeling in patients.[18,19] Currently, calcium channel blockers are mainly dihydropyridines, such as felodipine, nifedipine, and amlodipine. Studies have shown that the L-type calcium channel blocker felodipine can inhibit airway remodeling, thereby alleviating asthma.[20] Although some studies have reported good therapeutic effects of dihydropyridines, the application of these drugs is greatly hindered by side effects such as myalgia, arthralgia, headache, and cardiovascular issues. Additionally, due to individual differences and prolonged inhibition, dihydropyridines can lead to calcium channel blocker toxicity, resulting in bradycardia or even cardiogenic shock.[21] The genotype of α1 in the Cavα1 determines calcium ion channel subtypes, which are classified into three families: Cav1, Cav2, and Cav3. Cav2.3, a member of the Cav2 family corresponding to the R-type calcium channel, is primarily expressed in brain tissue and regulates neurotransmitter release. SNX-482 is a selective Cav2.3 inhibitor that is distinct from dihydropyridines. However, there have been no studies on SNX-482 in asthma, and existing research has mainly focused on its analgesic and sedative effects. Notably, a recent study showed that while SNX-482 inhibits Cav2.3 to alleviate postoperative pain in mice, it can also induce detectable side effects such as hyperactivity and reduced motor sensitivity, raising concerns about its safety.[22] Given that Cav2.3 mainly regulates neurotransmitter release, we speculate that Cav2.3 inhibitors could have a central antitussive effect to alleviate asthma. Currently, central antitussive drugs, such as codeine hydrochloride, are commonly used but are associated with unavoidable side effects, such as addiction and drowsiness. In conclusion, these findings suggest that inhibiting the calcium ion signaling pathway is an effective strategy for treating asthma, but there is an urgent need to develop safer and more effective Cav2.3 inhibitors for asthma treatment.

https://doi.org/10.2147/JIR.S579513

Ophiopogon japonicus (L. f). Ker Gawl. is a commonly used TCM with functions such as nourishing *yin*, generating body fluids, moistening the lungs, and relieving cough. It is often used to treat symptoms of lung and stomach *yin* deficiency, including thirst, dry cough, and hemoptysis.[23] Studies have reported that dwarf lilyturf root tuber can improve and prevent asthma by inhibiting the MAPK/NF-κB pathway.[24] Phytochemical research indicates that the main active component of dwarf lilyturf root tuber is ophiopogonin saponin.[25] Previous studies have shown that ophiopogonin saponins have various biological activities, including antitussive, anti-inflammatory, anti-asthma, and antioxidative effects.[25–27] For example, ophiopogonin D has been reported to ameliorate acute lung lesions by promoting STAT3-dependent A20 expression and ASK1 degradation, exhibiting strong anti-inflammatory activity.[28] Other studies have reported that ophiopogonin D can alleviate inflammation in alveolar epithelial cells by activating the AMPK/NF-κB pathway.[29] Notably, ophiopogonin D has demonstrated significant antitussive effects, primarily by inhibiting the depolarization of acetylcholine in airway paraneurons, selectively activating K-channels, and reducing parasympathetic control of airway function.[30] Formulas containing dwarf lilyturf root tuber, such as Ophiopogon decoction and Sha Radix Ophiopogon decoction, are widely reported to be used for treating cough caused by bronchitis, asthma, and pharyngitis.[31,32] These studies suggest that dwarf lilyturf root tuber and its active component ophiopogonin saponins, especially ophiopogonin D, have good therapeutic potential for alleviating asthma. Interestingly, our study found through molecular docking that DOA tightly binds to Cav2.3. The results revealed that DOA can target and bind Cav2.3 to inhibit the calcium ion signaling pathway and airway inflammation, marking the first report of DOA's potential as a therapeutic agent for asthma. It is worth noting that QRRZF has been used in clinical treatment for asthma for decades without any reported adverse effects, and there have been no reports of adverse effects associated with dwarf lilyturf root tuber itself. These results suggest that, compared to existing calcium channel blockers, DOA may have better safety. However, there is limited research on DOA, and further studies are needed to confirm its in vivo anti-asthma effects and elucidate the potential downstream molecular mechanisms through targeting Cav2.3 to alleviate asthma.

In summary, this study identified 21 components from QRRZF and selected DOA as the key active component, but the components of QRRZF remain to be fully identified. Moreover, there are still some limitations in this study: 1) Although CETSA confirmed the binding of DOA to Cav2.3, further experiments such as SPR, MST, and BLI are needed to assess the binding more thoroughly. 2) This study focuses only on the role of QRRZF and DOA in airway epithelial cells in HDM-induced allergic asthma. However, beyond classic type 2 asthma, studies have shown that airway epithelial cells also play important roles in the progression of non-type 2 and mixed asthma.;[33,34] therefore, future studies should also focus on the efficacy of QRRZF and DOA in non-type 2 asthma and mixed asthma. 3) Future studies should also include transcriptomics and proteomics to elucidate the downstream molecular mechanisms by which DOA targets and inhibits Cav2.3 to alleviate asthma. Collectively, DOA exerts its anti-asthma effects by targeting and binding Cav2.3, inhibiting the calcium signaling pathway and airway inflammation. This provides additional evidence for further research and clinical application of the QRRZF. However,

Conclusion

Overall, this study is the first to integrate UPLC-Q/TOF-MS/MS analysis, network pharmacology, and experimental validation to reveal the molecular mechanisms of QRRZF against asthma and identify DOA as the key active component. This study also preliminarily assessed the anti-asthma potential of DOA, providing a new potential therapeutic strategy for asthma.

Abbreviations

QRRZF, Qingre Runzao Formula; GEO, Gene Expression Omnibus; CETSA, Cellular Thermal Shift Assay; ICS, Inhaled Corticosteroids; LABA, Long-Acting β2-Agonists; HDM, House Dust Mite; 16HBE, Human Bronchial Epithelial cells; ZO-1, Zonula Occludens-1; BALF, Bronchoalveolar Lavage Fluid; Penh, Enhanced Pause; WBP, Whole-Body Plethysmography.

Data Sharing Statement

The datasets used during this study are available from the corresponding author upon reasonable request.

Ethics Approval and Consent to Participate

The human bronchial epithelial cells (16HBE cells) used in this study were commercially sourced, and human cDNA templates were prepared from 16HBE cells. Transcriptomic data for BA patients were obtained from the open-source GEO database. The animal research was conducted in strict accordance with ARRIVE 2.0 guidelines. Animal procedures were approved by the Animal Ethics Committee of Yunnan University of Chinese Medicine [approval number: R-062022G105], and were conducted in strict accordance with the China's national standard GB/T 35892-2018 Guidelines for Ethical Review of Laboratory Animal Welfare.

Author Contributions

Huan Li: Writing-original draft, Validation. Lingxue Jiang: Writing-original draft, Visualization, Validation. Jing Qian: Writing-original draft, Visualization, Validation. Wenping Bao: Writing-original draft, Data curation. Kenan Huang: Writing-original draft, Data curation. Dongyun Li: Writing-original draft, Methodology, Data curation. Aihua Zhang: Writing-review & editing, Methodology, Data curation. Jianguo Sun: Writing-review & editing, Visualization, Methodology, Validation. Jialong Lu: Writing-review & editing, Methodology, Data curation. Danxia Wei: Writing-review & editing, Methodology, Supervision, Funding acquisition, Conceptualization. All authors gave final approval of the version to be published, have agreed on the journal to which the article has been submitted, and agree to be accountable for all aspects of the work.

Funding

This study was supported by the National Natural Science Foundation of China (82260921), the Yunnan Provincial Ten-Thousand Talents Program (YNWR/MY/2020/08), and the Kunming Municipal Famous Traditional Chinese Medicine Expert Inheritance Studio Funding Program (MYGZS/2022/315).

Disclosure

All authors declare that there are no conflicts of interest in this work.

References

1. Savin IA, Zenkova MA, Sen'kova AV. Bronchial asthma, airway remodeling and lung fibrosis as successive steps of one process. *Int J Mol Sci*. 2023;24(22):16042. doi:10.3390/ijms242216042
2. Mattiuzzi C, Lippi G. Worldwide asthma epidemiology: insights from the global health data exchange database. *Int Forum Allergy Rhinol*. 2020;10(1):75–80. doi:10.1002/alr.22464
3. Huang K, Yang T, Xu J, et al. Prevalence, risk factors, and management of asthma in China: a national cross-sectional study. *Lancet*. 2019;394(10196):407–418. doi:10.1016/s0140-6736(19)31147-x
4. Reddel HK, Bateman ED, Schatz M, et al. A practical guide to implementing SMART in asthma management. *J Allergy Clin Immunol Pract*. 2022;10(1s):S31–s38. doi:10.1016/j.jaip.2021.10.011
5. Althoff MD, Holguin F. Care of the patient with asthma. *Ann Intern Med*. 2025;178(6):Itc81–itc96. doi:10.7326/annals-25-01034
6. Kuruvilla ME, Lee FE, Lee GB. Understanding asthma phenotypes, endotypes, and mechanisms of disease. *Clin Rev Allergy Immunol*. 2019;56(2):219–233. doi:10.1007/s12016-018-8712-1
7. Dabbs W, Bradley MH, Chamberlin SM. Acute asthma exacerbations: management strategies. *Am Fam Physician*. 2024;109(1):43–50.
8. Zhang C, D'Angelo D, Buttini F, et al. Long-acting inhaled medicines: present and future. *Adv Drug Deliv Rev*. 2024;204:115146. doi:10.1016/j.addr.2023.115146
9. Zhou B, Lu J, Chen Y, et al. Professor Lu Jialong's clinical experience in treating infantile cough with Qingre Runzao formula. *Chin J Ethnomedicine Ethnopharm*. 2023;32:56–58.
10. Yang H, Chen B, Wei D, et al. Clinical research on Qingre Runzao formula in treating dry cough in acute phase of chronic bronchitis. *Clin J Chin Med*. 2016;8:77–78. doi:10.3969/i.issn.1674-7860.2016.09.035
11. Zhao Q, Wu J, Yu W, et al. Experimental study on the effect of Qingre Runzao recipe on airway reaction and inflammatory reaction in asthmatic mice. *Shaanxi J Tradit Chin Med*. 2020;41:1695–1698+1707. doi:10.3969/i.issn.1000-7369.2020.12.004
12. Wu L, Hu X, Fu R, et al. Effect of Qingre Runzao oral liquid on chemokines and ILC2s and their upstream and downstream cytokines in asthmatic mice. *Chin J Comp Med*. 2021;31:1–9. doi:10.3969/j.issn.1671-7856.2021.09.001
13. Hu X, Wu L, Wei Y, et al. The impact of Qingre Runzao Oral Liquid on airway inflammation and airway mucus hypersecretion in asthmatic mice. *Chin Tradit Patent Med*. 2022;44:1281–1286. doi:10.3969/i.issn.1001-1528.2022.04.045
14. Jiashuo WU, Fangqing Z, Zhuangzhuang LI, et al. Integration strategy of network pharmacology in traditional Chinese medicine: a narrative review. *J Tradit Chin Med*. 2022;42(3):479–486. doi:10.19852/j.cnki.jtcm.20220408.003
15. Schoettler N, Strek ME. Recent advances in severe asthma: from phenotypes to personalized medicine. *Chest*. 2020;157(3):516–528. doi:10.1016/j.chest.2019.10.009

16. Wang MH, Chen C, Yeh ML, et al. Using traditional chinese medicine to relieve asthma symptoms: a systematic review and meta-analysis. *Am J Chin Med*. 2019;47(8):1659–1674. doi:10.1142/s0192415x1950085x
17. Jutel M, Agache I, Zemelka-Wiacek M, et al. Nomenclature of allergic diseases and hypersensitivity reactions: adapted to modern needs: an EAACI position paper. *Allergy*. 2023;78(11):2851–2874. doi:10.1111/all.15889
18. Chiu KY, Li JG, Lin Y. Calcium channel blockers for lung function improvement in asthma: a systematic review and meta-analysis. *Ann Allergy Asthma Immunol*. 2017;119(6):518–523.e513. doi:10.1016/j.anai.2017.08.013
19. Girodet PO, Dournes G, Thumerel M, et al. Calcium channel blocker reduces airway remodeling in severe asthma. A proof-of-concept study. *Am J Respir Crit Care Med*. 2015;191(8):876–883. doi:10.1164/rccm.201410-1874OC
20. Patel KR, Peers E. Felodipine, a new calcium antagonist, modifies exercise-induced asthma. *Am Rev Respir Dis*. 1988;138(1):54–56. doi:10.1164/ajrccm/138.1.54
21. Hazra PK, Mehta A, Desai B, et al. Long-acting nifedipine in the management of essential hypertension: a review for cardiologists. *Am J Cardiovasc Dis*. 2024;14(6):396–413. doi:10.62347/rpmz6407
22. Ferreira MA, Lückemeyer DD, Martins F, et al. Pronociceptive role of spinal Ca(v)2.3 (R-type) calcium channels in a mouse model of postoperative pain. *Br J Pharmacol*. 2024;181(19):3594–3609. doi:10.1111/bph.16407
23. Chen MH, Chen XJ, Wang M, et al. Ophiopogon japonicus--A phytochemical, ethnomedicinal and pharmacological review. *J Ethnopharmacol*. 2016;181:193–213. doi:10.1016/j.jep.2016.01.037
24. Lee I-S, Kim D-H, Kim K-H, et al. Prevention and relaxation effects of Liriope platyphylla on bronchial asthma in vitro model by suppressing the activities of MAPK/NF-κB pathway. *Mol Cellular Toxicol*. 2019;15(3):325–334. doi:10.1007/s13273-019-0036-6
25. Lei F, Weckerle CS, Heinrich M. Liriopogons (genera ophiopogon and liriope, asparagaceae): a critical review of the phytochemical and pharmacological research. *Front Pharmacol*. 2021;12:769929. doi:10.3389/fphar.2021.769929
26. An EJ, Kim Y, Lee SH, et al. Ophiopogonin D ameliorates DNCB-induced atopic dermatitis-like lesions in BALB/c mice and TNF-α- inflamed HaCaT cell. *Biochem Biophys Res Commun*. 2020;522(1):40–46. doi:10.1016/j.bbrc.2019.10.190
27. Wang L, Yang H, Qiao L, et al. Ophiopogonin D inhibiting epithelial NF-κB signaling pathway protects against experimental colitis in mice. *Inflammation*. 2022;45(4):1720–1731. doi:10.1007/s10753-022-01655-8
28. Shen X, Ruan Y, Zhao Y, et al. Ophiopogonin D alleviates acute lung injury by regulating inflammation via the STAT3/A20/ASK1 axis. *Phytomedicine*. 2024;130:155482. doi:10.1016/j.phymed.2024.155482
29. Wang Y, Li D, Song L, et al. Ophiopogonin D attenuates PM2.5-induced inflammation via suppressing the AMPK/NF-κB pathway in mouse pulmonary epithelial cells. *Exp Ther Med*. 2020;20(6):139. doi:10.3892/etm.2020.9268
30. Ishibashi H, Mochidome T, Okai J, et al. Activation of potassium conductance by ophiopogonin-D in acutely dissociated rat paratracheal neurones. *Br J Pharmacol*. 2001;132(2):461–466. doi:10.1038/sj.bjp.0703818
31. Lao Q, Wang X, Zhu G, et al. A Chinese classical prescription Maimendong decoction in treatment of pulmonary fibrosis: an overview. *Front Pharmacol*. 2024;15:1329743. doi:10.3389/fphar.2024.1329743
32. Aizawa H, Shigyo M, Nakano H, et al. Effect of the Chinese herbal medicine, Bakumondo-to, on airway hyperresponsiveness induced by ozone exposure in Guinea-pigs. *Respirology*. 1999;4(4):349–354. doi:10.1046/j.1440-1843.1999.00203.x
33. Potaczek DP, Miethe S, Schindler V, et al. Role of airway epithelial cells in the development of different asthma phenotypes. *Cell Signal*. 2020;69:109523. doi:10.1016/j.cellsig.2019.109523
34. Tan HT, Hagner S, Ruchti F, et al. Tight junction, mucin, and inflammasome-related molecules are differentially expressed in eosinophilic, mixed, and neutrophilic experimental asthma in mice. *Allergy*. 2019;74(2):294–307. doi:10.1111/all.13619